A fast and stable calibration method for VLP system without any geometric measurement

Tianming Huang[1], Yuan Zhuang[1,2], Xiansheng Yang[1], Xiao Sun[1]

[1] State Key Laboratory of Information Engineering in Surveying, Mapping and Remote Sensing, Wuhan University, Wuhan 430072, China - huangtianmingw@outlook.com, (xiansheng.yang, xsun, yuan.zhuang)@whu.edu.cn
[2] Luojia Laboratory and the Wuhan Institute of Quantum Technology, Wuhan 430072, China - yuan.zhuang@whu.edu.cn

Keywords: Visible light positioning (VLP), Calibration, Lambert model, Received signal strength (RSS), Photo-detector (PD).

Abstract

Visible light positioning (VLP) is one of the most promising technologies for providing high-precision, low-cost indoor positioning and navigation services. However, the traditional calibration methods of VLP are complex and unfriendly to users, which hinders the large-scale commercial deployment of VLP systems. In this letter, a fast and stable calibration method for Lambert model in the received signal strength (RSS)-based VLP system is proposed, which dispenses with geometric measurement and greatly simplifies the calibration procedures. The proposed method calibrates the Lambert model through two steps, firstly using a ratio method to calibrate the Lambert order, and then estimating the constant term. The actual processes only require moving a robot equipped with a photo-detector (PD) along a rectangular trajectory once, and then the program will automatically estimate the required parameters by analyzing the RSS during this period. Experimental results show a good stability of the calibrated parameters, as well as a excellent distance measuring accuracy within 12 cm. And the entire processes, including signal collection and processing, only take a total of no more than four minutes.

1. Introduction

Location based services (LBS) are becoming increasingly important in indoor scenes, such as parking lots, logistics centers, and smart shopping malls, where the radio frequency (RF) based global navigation satellite system (GNSS) does not performs well since signals are easily obstructed [Bastiaens et al., 2024]. Therefore, several indoor positioning systems (IPSs) such as wireless local area network (WLAN), bluetooth low energy (BLE), acoustic tag, ultra-wideband (UWB) and visible light positioning (VLP) have been proposed [Lin et al., 2024, Huang et al., 2023]. Compared with other IPSs, most VLP systems has been demonstrated with a high accuracy and low cost [Guan et al., 2020, Abou-Shehada et al., 2021, Chen et al., 2021]. What is more, they have the advantages of immunity to RF-induced electromagnetic interference, a free and unrestricted spectrum, and a much higher level of security at the physical layer [Fang et al., 2023, Yang et al., 2020].

The VLP systems usually use several LEDs as its transmitters (Txs) and a photo-detector (PD) or an image sensor (IS) as its receiver (Rx) [Zhuang et al., 2018]. Because of the low frame rate and small field of view (FoV), the IS-based VLP systems usually have a poor robustness and mobility. Even worse, the Rx camera may threaten the privacy of the users. PD-based VLP systems usually estimate the distances between the Rx and the Txs by a channel model, mostly the Lambert model, and then calculate the Rx position by the trilateration method. The unknown parameters for the Lambert model should be calibrated before running the VLP system [Zhuang et al., 2018, Maheepala et al., 2020]. The traditional methods calibrated the Lambert model have complex processes [Yang et al., 2023]. Firstly, it is necessary to select some calibration points (CPs) that are evenly distributed from close to far to ensure a more universal fitting result. Meanwhile, the RSS of all these CPs should be measured as well calculating the distances from each CP to each LED. Then, they can use linear least squares to fit the logarithms of distances and RSS in the Lambert model [Hua et al., 2021]. The traditional calibration processes of Lambert models not only require a lot of measurement work, but also have a certain learning cost, which makes it difficult to promote VLP systems in real life. Therefore, a simple, fast, and user-friendly calibration method is important for the industrialization of VLP systems.

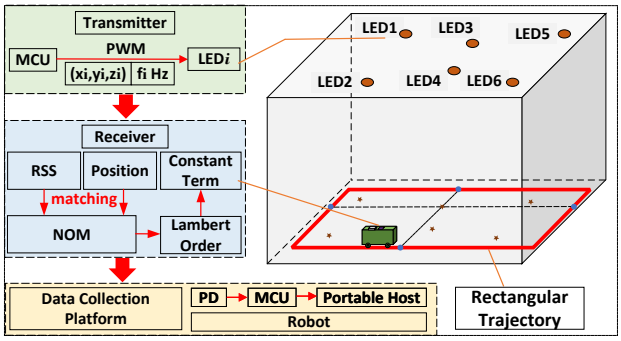

Figure 1. Framework of the proposed calibration method.

In this letter, we propose a fast and stable calibration method of the Lambert model for VLP system without any geometric measurement. As is shown in Fig. 1, we use a robot to drive the Rx moving along a rectangular trajectory around the LEDs, while continuously measuring RSS using a PD. Because each LED has been modulated by a micro-controller unit (MCU) with a pulse width modulation (PWM) wave at a unique frequency, we use a band pass filter (BPF) to process the RSS to get the timing RSS of each LED during this period. We propose a solution to match the processed RSS with the geometric position on the rectangular trajectory. Based on the matching relationship, we finally estimate the Lambert order through a nonlinear optimization model (NOM), and further calculate the constant term. Experimental results show a good consistence of the calibration parameters of three different routes and mean distance measurement error < 12 cm. And the entire calibration processes, including signal collection and processing, only

take a total of no more than four minutes.

The rest of the letter is organized as follows: in Section II, the channel model and the two-step calibration approach is proposed. Sections III presents the procedures of the proposed calibration method, and Sections IV shows the experiments and results. Finally, Section V summarizes the conclusions.

2. Channel Model

Assuming that the LED is a Lambert light source, the light of sigh (LOS) transmission channel gain of the visible light from the LED to the PD can be expressed as [Zhuang et al., 2018]:

$$H(0) = \begin{cases} \frac{AT(\Psi)g(\Psi)(m+1)}{2\pi d^2}\cos^m(\phi)\cos(\Psi), & 0 \le \Psi \le \Psi_c \\ 0, & \Psi > \Psi_c \end{cases} \tag{1}$$

where d=distance from the LED to the PD
A= effective photoelectric effect area of the PD
ϕ = radiation angle
Ψ =incident angle
$T(\Psi)$=optical filter gain
$g(\Psi)$= optical concentrator gain
m = Lambert order

Assuming that P_t represents the LED emission power, through the channel propagation, the received power P_r of the PD is:

$$P_r = P_t H(0). \tag{2}$$

The P_r can further expressed as:

$$P_r = \frac{(m+1)AP_t}{2\pi d^2} T_s(\Psi) g(\Psi) \cos^m(\phi)\cos(\Psi). \tag{3}$$

Note that in the absence of a lens between the LED and the PD, $T_s(\Psi)$ and $g(\Psi)$ are both 1. When both the LED and PD are placed horizontally, there will be $\cos(\Psi) = \cos(\phi) = h/d$. Since $P_r \propto RSS$, Eq. (3) can be represent as:

$$RSS = \frac{a(m+1)h^{m+1}}{d^{m+3}}, \tag{4}$$

where a = simplified constant term

The traditional calibration methods usually take a logarithm of both sides of Eq. (4) and then linearly fit it. It may lead to a problem where the constant term a and exponential term interact with each other and fluctuate greatly in several consecutive tests. In order to reduce the influence on the constant term a and better fit m, we propose a ratio fitting method. We substitute two test-points into the Eq. (4), and get the ratio of the both sides:

$$RSS_1/RSS_2 = d_2^{m+3}/d_1^{m+3}. \tag{5}$$

And then take the logarithm of both sides of the Eq. (5), there will be:

$$log(RSS_1/RSS_2) = (m+3)log(d_2/d_1). \tag{6}$$

The Eq. (6) is a form of proportional function, where the coefficient $(m+3)$ is easily fitted by using a linear least square

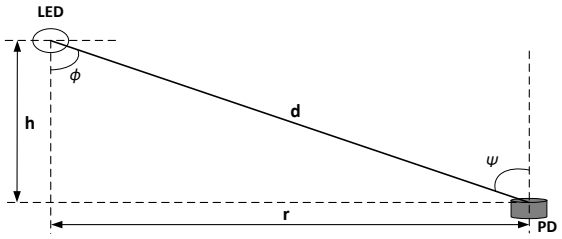

Figure 2. Geometric model of LOS transmission

method with by several test-points. After that, we estimate a by that test-points. Using n represents the number of these test-points, there will be:

$$a = \frac{1}{n}\sum_{i=1}^{n} \frac{RSS_i d_i^{m+3}}{(m+1)h_i^{m+1}}. \tag{7}$$

Finally, we estimate the two required parameters a and m in Eq. (4).

3. Calibration Method

In this letter, we propose a fast and robust method to calibrate the Lambert model, which is unnecessary to take any geometric measurement. It means that we can not directly use Eq. (6) and (7) to estimate the unknown parameters a and m, because the parameters d and h are also unknown. In order to establish more geometric relationship between the positions and RSS of the Rx, the proposed method requires moving the Rx along a rectangular trajectory once, and then estimates the required parameters by analyzing the RSS during this period.

3.1 RSS Collection and Processing

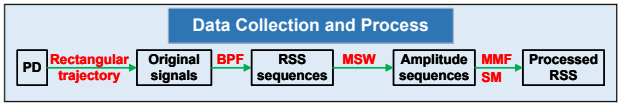

Figure 3. The block diagram of the procedures of RSS collection and processing.

Fig. 3 shows the block diagram of the procedures of the RSS collection and processing. Firstly, we use a robot to drive the Rx moving along a rectangular trajectory around the LEDs, while continuously measuring RSS using a PD that is the only one sensor required in this method, the original signals of the output of the PD is shown in Fig. 4(a). Secondly, we use a BPF to process the RSS since each LED works at a unique frequency. Then we get the timing RSS sequences of each LED, which has a temporal resolution of $1/fs$, where fs is the sample rate of PD. Because of the original modulated signal of each LED is a PWM wave, we find the maximum of a appropriately sized sliding window (MSW) as the amplitude of the PWM signal during this period. Then we get the amplitude sequences of each LED as shown in Fig. 4(b). A moving mean filter (MMF) and a quadratic polynomial fitting-based smoother (SM) will be used to smooth the amplitude sequences to get the processed RSS of each LED that are shown in Fig. 4(c).

3.2 Matching RSS with Position

Fig. 4(a) and (b) show the dynamic changes of the RSS of each LED over time. According to Eq. (4), the distance from the

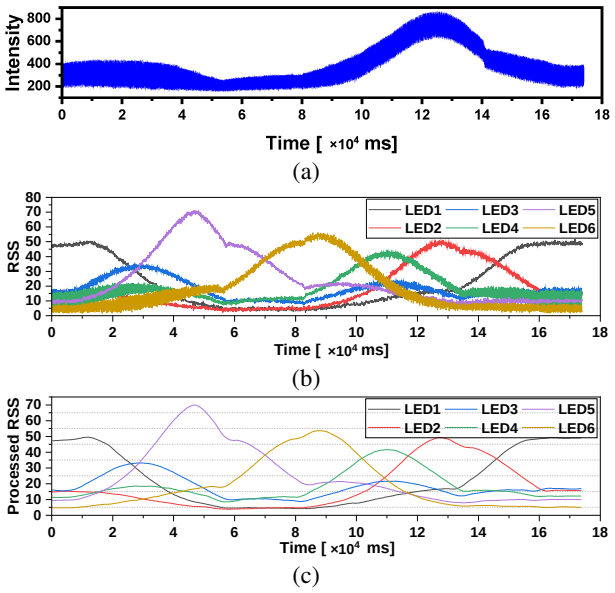

Figure 4. Data Processing: (a) the original signals, (b) the amplitude sequences, and (c) the processed RSS.

PD to each LED changing all the time when the robot moves through the vertices A, B, C, D and A of the rectangular trajectory successively as shown in Fig. 5(a). There is the expression of d_i that is the distance from the PD to each LED:

$$d_i = \left|P\vec{L}_i\right| = \begin{cases} \sqrt{(x_i - x_a)^2 + (y_i - y)^2 + h^2}, & P \epsilon AB \\ \sqrt{(x_i - x)^2 + (y_i - y_c)^2 + h^2}, & P \epsilon BC \\ \sqrt{(x_i - x_c)^2 + (y_i - y)^2 + h^2}, & P \epsilon CD \\ \sqrt{(x_i - x)^2 + (y_i - y_a)^2 + h^2}, & P \epsilon DA \end{cases} \tag{8}$$

where P represents the position of PD whose coordinates are (x, y), and L_i is the position of i-th LED with the coordinates of (x_i, y_i). The height difference between PD and the plane of LEDs is expressed as h, which is a constant. We assume that the coordinates of the two vertices A and C are (x_a, y_a) and (x_c, y_c). We can observe that each segment of a piecewise function contains only one variable. when $P \epsilon AB$, d_i has the minimum value at $y = y_i$. P_1 is used to represent the position of P at this moment with the coordinates of (x_a, y_i). Similarly, d_i has the minimum value when P at the position of P_2, P_3 and P_4 in each segmented interval BC, CD and DA with the coordinates of (x_i, y_c), (x_c, y_i) and (x_i, y_a), respectively. According to Eq. (4), RSS increases as d decreases. Therefore, RSS has the maximum value in each segmented interval when P at the position of P_1, P_2, P_3 and P_4. Fig. 5(b) shows the RSS of LED3 change over time, where T_1, T_2, T_3 and T_4, respectively, present the time when the robot moves through the vertices B, C, D, A successively.

Assuming that there are N LEDs, the maximum point of the RSS in each segmented interval of each LED can be expressed as:

$$[v_{ij}, t_{ij}] = max(\mathbf{RSS}_i(t)),\ t \epsilon (T_{j-1}, T_j) \tag{9}$$

where v_{ij} and t_{ij} represent the RSS value and its time of the i-th LED in the j-th segmented interval. $\mathbf{RSS}_i(t)$ is the function of the i-th LED RSS with time t, and $i = \{1, 2, ..., N\}$, $j = \{1, 2, 3, 4\}$. At the time of t_{ij}, the RSS values of all N LEDs can be found, which are:

$$\mathbf{RSS}(t_{ij}) = \{RSS_i(t_{ij}), i = \{1, 2, ..., N\}\} \tag{10}$$

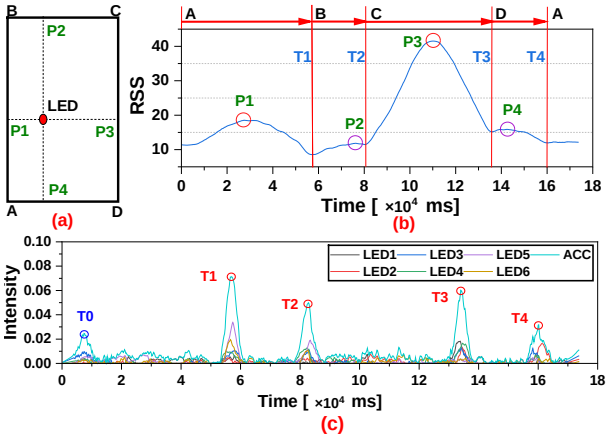

Figure 5. Signal processes: (a) the designed rectangular trajectory, (b) RSS of LED3, and (c) the second-order derivative of each LED after zeroing and its sum sequences.

where i-th LED RSS can be regarded as $RSS_i(t_{ij})$. We can also express the coordinates of the PD at the time of t_{ij}:

$$P_{ij} = \begin{cases} (x_a, y_i), & j = 1 \\ (x_i, y_c), & j = 2 \\ (x_c, y_i), & j = 3 \\ (x_i, y_a), & j = 4 \end{cases} \tag{11}$$

By Eq. (9), (10) and (11), we can get a matching relationship that PD located on P_{ij} can get the RSS values of $\mathbf{RSS}(t_{ij})$ from all LEDs at the time t_{ij}.

3.3 Determine Vertex Time

If we express the d_i as the function of time t, there will be:

$$d_i(t) = \begin{cases} \sqrt{(x_i - x_a)^2 + (y_i - y(t))^2 + h^2}, & t \epsilon (0, T_1) \\ \sqrt{(x_i - x(t))^2 + (y_i - y_c)^2 + h^2}, & t \epsilon (T_1, T_2) \\ \sqrt{(x_i - x_c)^2 + (y_i - y(t))^2 + h^2}, & t \epsilon (T_2, T_3) \\ \sqrt{(x_i - x(t))^2 + (y_i - y_a)^2 + h^2}, & t \epsilon (T_3, T_4) \end{cases} \tag{12}$$

I is very easily to find that d_i is a continuous function of time t because of the following relationship at the time of each vertex:

$$d_i(T_j^-) = d_i(T_j) = d_i(T_j^+), \quad j = \{1, 2, 3, 4\}. \tag{13}$$

Clearly, $d_i(t)$ increases monotonically on $(T_j - \Delta t, T_j)$ and decreases monotonically on $(T_j, T_j + \Delta t)$, where $(T_j - \Delta t, T_j + \Delta t)$ is a smaller interval around T_j. Thus, $d_i(t)$ has a maximum point at T_j and RSS has a minimum point at T_j. We have designed a algorithm to determine the vertex time T_j. Firstly, we use a MMF to process the amplitude sequences in Fig. 4(a). Since the second derivative is adept at identifying minimum points, we apply the derivative operation to the MMF output twice. Before each derivation, we employ the SM to mitigate noise effects on the derivative calculation. If the value of one second-order derivative < 0, set its value as 0, as the second-order derivative at a minimum point should be > 0. Fig. 5(c) shows the second-order derivative of each LED after zeroing. Next, we accumulate the second derivatives of each LED to obtain a second-order derivative sum sequences, represented as 'ACC' in Fig. 5(c). The graph reveals four prominent peaks, which correspond to vertex times T_1, T_2, T_3 and T_4, respectively. Additionally, another prominent peak appears at the be-

ginning of the graph, denoted as T_0. This peak is caused by the robot shaking when it abruptly starts moving from a stationary position, causing the PD to tilt and resulting in a sudden RSS decrease. As the robot stabilizes, the PD returns to a relatively horizontal state. Therefore, T_0 actually is the exact start time of the robot.

3.4 Parameters Estimation by Nonlinear Optimization

When we determined the vertex time T_1, T_2, T_3 and T_4, we find the v_{ij} and t_{ij} using Eq. (9). Then, we get the $\mathbf{RSS}(t_{ij})$ and P_{ij} using Eq. (10) and (11). Finally, we get a position matrix $\mathbf{P}$ and a signal matrix $\mathbf{RSS}$, which are made up of $4N$ P_{ij} and $\mathbf{RSS}(t_{ij})$. We establish a NOM that use both the $\mathbf{P}$ and $\mathbf{R}$ to estimate the Lambert order of each LED, according to Eq. (6). If the distance from P_{ij} to the i-th LED is d_{ij} and the RSS_{ij} is the RSS value of the i-th LED when PD is at P_{ij}, the objective function f of the NOM can be expressed as:

$$f = \sum_{i=1}^{N} \sum_{j=1}^{4N} w(i,j)(log\frac{RSS_{i1}}{RSS_{ij}} - (m_i+3)log\frac{d_{ij}}{d_{i1}})^2. \quad (14)$$

The solver of the objective function f is:

$$S = arg\min_{s \to s_0} f, \quad (15)$$

where m_i means the Lambert order of i-th LED and $w(i,j)$ means the weight of RSS_{ij}. When we carefully compare Fig. 5(a) and Fig. 5(b), we will find that the positions P_2 and P_4 in Fig. 5(b) are unreasonable. This is because when the signal-to-noise ratio (SNR) is low, the maximum value may not necessarily correspond exactly to its position. Therefore, we set a certain threshold TH here to filter the lower RSS values. When it less than TH, $w(i,j) = 0$. There are $4+1+N$ unknown parameters in the objective function, which are constrained in a certain range. So we choose the Sequential Quadratic Programming (SQP) algorithm to solve this constrained optimization problems [Curtis and Overton, 2012]. The main idea of the SQP algorithm is to transform nonlinear optimization problems into a series of quadratic programming sub-problems, and approach the global optimal solution by solving these sub-problems, as Algorithm 1 shown. After estimating m, the constant term a can be calculated by substitute m into the Eq. (7).

Algorithm 1 Nonlinear Optimization Model.

INPUT
  $\mathbf{RSS}$ $(N \times 4N)$
OUTPUT
  $\{m_i, a_i\ ,\ i = 1, 2, ..., N\}$
PARAMETERS
  $\{m_i, a_i\ ,\ i = 1, 2, ..., N,\ x_a, y_a, x_c, y_c, h\}$
OBJECTIVE FUNCTION
  for $\mathbf{i = 1 : 1 : N}$
    for $\mathbf{j = 1 : 1 : 4N}$
    if($\mathbf{RSS_{ij} < TH}$) $\mathbf{w(i,j) = 0}$
    else $\mathbf{w(i,j) = 1}$
    end
    $\mathbf{d_{ij}} = \left|\overrightarrow{P_{ij}L_i}\right|$
    $\mathbf{f \leftarrow Eq.(14)}$
    end
  end
SOLVER
  $\mathbf{S \overset{SQP}{\leftarrow} Eq.(15)}$

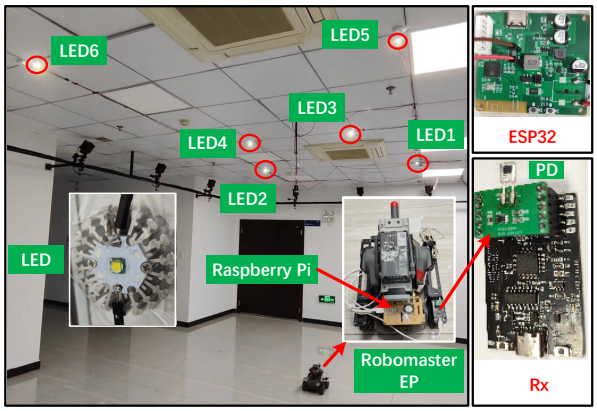

Figure 6. Hardwares system.

4. Experiments and Results

4.1 Experimental Environments

Fig. 6 is the test environment, where 6 LEDs are fixed on the ceiling at a height of $2.8m$. The Tx of each LED is made up of the ESP32 MCU operating at a specific frequency and with a direct-current (DC) power supply. The Rx integrated a PD and STM32 MCU powered by a portable host Raspberry Pi, which also have a data access to the Rx. Both the Rx and the Raspberry Pi are fixed on Robomaster EP, which has come up of a mobile wireless data collection platform. The detachable battery provides power for the robot and the Raspberry Pi. All the key experimental parameters are given in Table 1.

Table 1. Experimental Parameters

Parameters	Values
LED voltage / V	14
Frequencies of LEDs / Hz	$(157, 289, 437, 589, 777, 943)$
Coordinates of LEDs / m	$(1.37, 1.65), (3.73, 1.62)$ $(1.96, 3.38), (3.19, 3.40)$ $(1.35, 5.19), (3.69, 5.79)$
Height of LEDs / m	2.8
Sample rate of PD / kHz	2
Size of room /m^2	5.5×8

We have verified the proposed method by four aspects including the time cost, parameters stability, performance of distance measurement and positioning accuracy. As a comparison, we have also manually measured the RSS values and positions of 12 CPs to estimate the parameters using the traditional calibration method (Trad). The Robomaster EP is programmed to move on three different rectangular trajectories (Trajs).

4.2 Stability

The calibrated results of the proposed method are shown in Table 2 and Table 3. In Table 2, the m of all LEDs are from 0 to 0.27, and LED1 has the largest variation, reaching 0.13, while other LEDs have smaller fluctuations. When we put the maximum and minimum of m of LED in Eq.4, and set the same value of other parameters, we find the relative change of the RSS is very small. It means that the Lambert orders of each LED in three trajectories are stable. Table 3 shows the differences in a of each LED, but the fluctuation of a of each LED in the three trajectories is small. LED3 has the largest variation with 21, which is 7 percent of the maximum of 300. The difference in a for other LEDs is smaller that stands the calibrated constant terms of all LEDs are consistency.

Table 2. Calibrated Lambert order

Trajs	LED1	LED2	LED3	LED4	LED5	LED6
traj 1	0.27	0.13	0	0.08	0.18	0
traj 2	0.14	0.08	0	0.09	0.19	0
traj 3	0.14	0.06	0	0.09	0.11	0.02

Table 3. Calibrated constant term

Trajs	LED1	LED2	LED3	LED4	LED5	LED6
traj 1	282	298	298	298	340	319
traj 2	292	297	277	278	320	300
traj 3	297	307	290	278	340	296

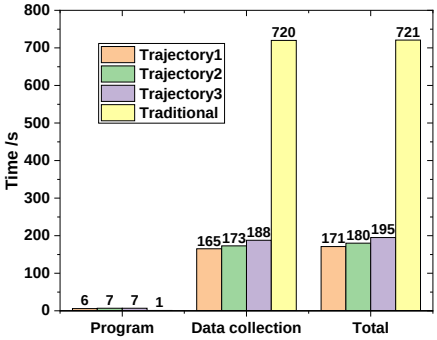

Figure 7. Time cost of different trajectories and different project.

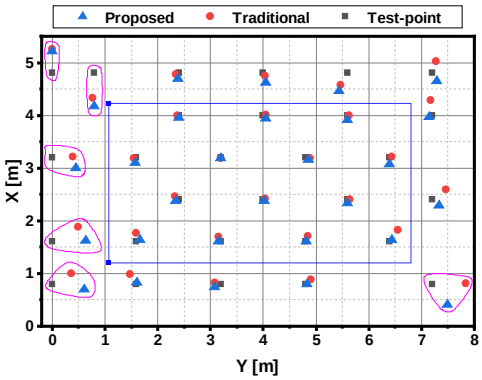

Figure 8. static test for VLP by some test-points.

4.3 Time Cost

We recorded the total time required for the proposed calibration method on three different trajectories, including data collection and program running time. As a comparison, we also recorded the time required for traditional methods, where the data collection time for each CP is approximately one minute, and the 12 CPs take 12 minutes. From Fig. 7, the proposed calibration method is faster, and the entire processes, including signal collection and processing, only takes a total of no more than four minutes. Users for traditional method have to spend much time to learn how to correctly choose CPs and some other procedures. If we take the learning cost into consideration, the proposed method are more efficient because of its almost automated program.

4.4 Distance Measurement Performance

In order to test the performance of distance measurement using the calibrated parameters in Table 2 and Table 3, we have selected some test-points (TPs) in the central area of the room (inside the blue rectangle in the graph) and the edge area within

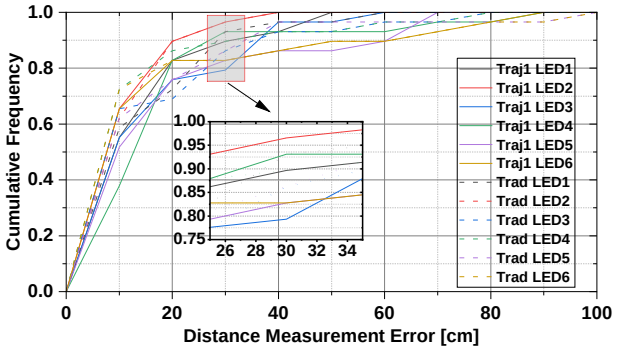

Figure 9. CDF of the distance measurement errors.

1 meter from the wall as shown in Fig. 8. The result of the mean error (ME) of distance measurement of each LED is shown in Table 4 and 5. We find that in the central areas, the MEs of each LED in all trajectories are at a level of less than 12 cm, while it less than 40 cm in the edge areas of the room. The main reason is that the measured RSS are severely influenced by the reflected lights in the edge areas of the room. It can be seen that the traditional method has a better accuracy in all LED in the central areas. This may be because all the three rectangular trajectories we designed did not pass through the central areas. Even though we also has a good accuracy of each LED in the central areas. In the edge areas, the proposed method has a roughly the same level of accuracy with the traditional method. We have calculated the cumulative distribution function (CDF) of all the TPs both in central and edge areas and plot them in Fig. 9, from which we also find that the proposed method has similar performance of distance measurement with traditional methods, and all LEDs in trajectory 1 have a less than 31 cm with a confidence level of 0.8.

Table 4. Distance measuring performance in central areas [cm]

Trajs	LED1	LED2	LED3	LED4	LED5	LED6
Traj 1	7.6	6.5	5.0	11.9	5.4	5.9
Traj 2	5.1	6.8	10.3	5.0	8.8	4.4
Traj 3	5.5	6.0	6.4	4.9	7.0	4.6
Trad	4.6	6.1	4.5	2.9	4.4	3.0

Table 5. Distance measuring performance in edge areas [cm]

Trajs	LED1	LED2	LED3	LED4	LED5	LED6
Traj 1	19.4	11.6	22.3	20.3	27.0	26.0
Traj 2	19.4	13.1	26.4	17.0	28.6	27.0
Traj 3	19.0	12.9	23.6	17.0	27.2	27.3
Trad	18.8	14.2	23.1	18.9	23.6	25.3

4.5 Positioning Accuracy

The static positioning performance has also been verified by using the calibrated parameters in Table 2 and Table 3, and the results are also shown in Fig. 8. Fig. 8 shows the 2D positioning performance of both the proposed and traditional methods, from which we gte the conclusion that both have excellent performance, except for some TPs closely attached to the wall (circled in red). We have also calculated the CDF of all the TPs both in central and edge areas and plot them in Fig. 9, from which we also find that the proposed method has similar performance of positioning accuracy with traditional methods. The CDF curves of the proposed method rises rapidly in the early stage and is relatively flat in the later stage. This indicates that the positioning errors of the proposed method are more polarized, reflecting a higher positioning accuracy in the central

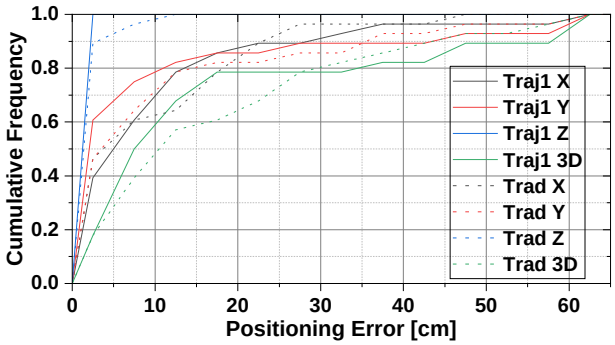

Figure 10. Cumulative distribution function of the positioning errors.

ares but a severe performance degradation at the edges due to the influence of reflected light.

The stability of the proposed method can be seen from the small differences in the parameters calibrated by three different trajectories. Compared to traditional methods, one-third of the time cost reflects the speed advantage of the proposed method. The distance measuring and positioning accuracy represent that the proposed calibration method for RSS-based VLP system has a good performance.

5. Conclusions

In this letter, we have proposed a fast and highly stable calibration method for RSS-based VLP system. Compared with the traditional calibration methods that are complex and unfriendly to users, the proposed calibration method is unnecessary to take any geometric measurement and greatly simplifies the calibration procedures. It only requires moving the receiver along a rectangular trajectory once, and then automatically estimating the required parameters by matching the positions with the RSS during this period. We have implemented a fully automated calibration processes, allowing users to have almost no learning cost. Experimental results show a high consistence and stability of the calibrated parameters in different trajectories, as well as a excellent distance measuring accuracy with the level of less than 12 cm in the central areas of the floor. And the entire processes, including signal collection and processing, only take a total of no more than four minutes. In the future, the proposed method can be used for rapid access to indoor VLP systems for high-precision positioning when unmanned aerial vehicles (UAV) enter indoor scenes. In addition, it will be beneficial for the large-scale commercialization of VLP systems.

References

Abou-Shehada, I. M., AlMuallim, A. F., AlFaqeh, A. K., Muqaibel, A. H., Park, K.-H., Alouini, M.-S., 2021. Accurate Indoor Visible Light Positioning Using a Modified Pathloss Model With Sparse Fingerprints. *Journal of Lightwave Technology*, 39(20), 6487-6497.

Bastiaens, S., Alijani, M., Joseph, W., Plets, D., 2024. Visible Light Positioning as a Next-Generation Indoor Positioning Technology: A Tutorial. *IEEE Communications Surveys & Tutorials*.

Chen, H., Han, W., Wang, J., Lu, H., Chen, D., Jin, J., Feng, L., 2021. High accuracy indoor visible light positioning using a long short term memory-fully connected network based algorithm. *Optics Express*, 29(25), 41109–41120.

Curtis, F. E., Overton, M. L., 2012. A sequential quadratic programming algorithm for nonconvex, nonsmooth constrained optimization. *SIAM Journal on Optimization*, 22(2), 474–500.

Fang, J., Pan, J., Huang, X., Lin, J., Jiang, C., 2023. Integrated physical-layer secure visible light communication and positioning system based on polar codes. *Optics Express*, 31(25), 41756–41772.

Guan, W., Chen, S., Wen, S., Tan, Z., Song, H., Hou, W., 2020. High-Accuracy Robot Indoor Localization Scheme Based on Robot Operating System Using Visible Light Positioning. *IEEE Photonics Journal*, 12(2), 1-16.

Hua, L., Zhuang, Y., Li, Y., Wang, Q., Zhou, B., Qi, L., Yang, J., Cao, Y., Haas, H., 2021. FusionVLP: The fusion of photodiode and camera for visible light positioning. *IEEE Transactions on Vehicular Technology*, 70(11), 11796–11811.

Huang, T., Lin, B., Ghassemlooy, Z., Jiang, N., Lai, Q., 2023. Three-Dimensional NLOS VLP Based on a Luminance Distribution Model for Image Sensor. *IEEE Internet of Things Journal*, 10(8), 6902-6914.

Lin, X., Chen, R., Huang, L., Liu, Z., Niu, X., Guo, G., Li, Z., Qian, L., 2024. ChirpTracker: A Precise-Location-Aware System for Acoustic Tag Using Single Smartphone. *IEEE Internet of Things Journal*, 11(1), 848-862.

Maheepala, M., Kouzani, A. Z., Joordens, M. A., 2020. Light-Based Indoor Positioning Systems: A Review. *IEEE Sensors Journal*, 20(8), 3971-3995.

Yang, H., Zhong, W.-D., Chen, C., Alphones, A., 2020. Integration of Visible Light Communication and Positioning within 5G Networks for Internet of Things. *IEEE Network*, 34(5), 134-140.

Yang, X., Zhuang, Y., Shi, M., Sun, X., Cao, X., Zhou, B., 2023. RatioVLP: Ambient Light Noise Evaluation and Suppression in the Visible Light Positioning System. *IEEE Transactions on Mobile Computing*.

Zhuang, Y., Hua, L., Qi, L., Yang, J., Cao, P., Cao, Y., Wu, Y., Thompson, J., Haas, H., 2018. A Survey of Positioning Systems Using Visible LED Lights. *IEEE Communications Surveys and Tutorials*, 20(3), 1963-1988.